Radio Imaging With SWAN*

Satyapan Munshi

The Indian SWAN (Sky Watch Array Network) is a radio interferometric array presently located at Gauribidanur, near Bengaluru and operated by the Raman Research Institute. The primary motive behind the SWAN initiative is to provide much-needed exposure to research in radio astronomy to undergraduates interested in this field. At the same time, the SWAN is expected to increase Indian observing capabilities at low radio frequencies significantly. This article introduces imaging in radio astronomy and the corresponding data analysis techniques I learned while being associated with the SWAN project.

Satyapan Munshi is an undergraduate student at IISER Mohali, majoring in physics. He is interested in pursuing research in astrophysics.

1. Introduction

Radio astronomy studies astronomical sources that emit electromagnetic waves in radio frequencies (roughly from 10 MHz to 1 THz). It is one of the several fields of science which received a significant boost due to the technology developed as a part of the operations of the Second World War. Though astronomy is one of the oldest sciences, it wasn't until a mere century back that humans started exploring the field of radio astronomy when scientists successfully measured parts of the electromagnetic spectrum outside the optical regime. In the years that followed, radio astronomy quickly became one of the most active fields of astronomical research and has contributed significantly to our present understanding of the universe.

This article introduces imaging in radio astronomy utilizing the work I did as an undergraduate while being associated with the SWAN. The SWAN project is also introduced to the readers since

Keywords
Radio astronomy, radio telescopes, interferometry, data analysis.

*Vol.27, No.8, DOI: https://doi.org/10.1007/s12045-022-1428-9

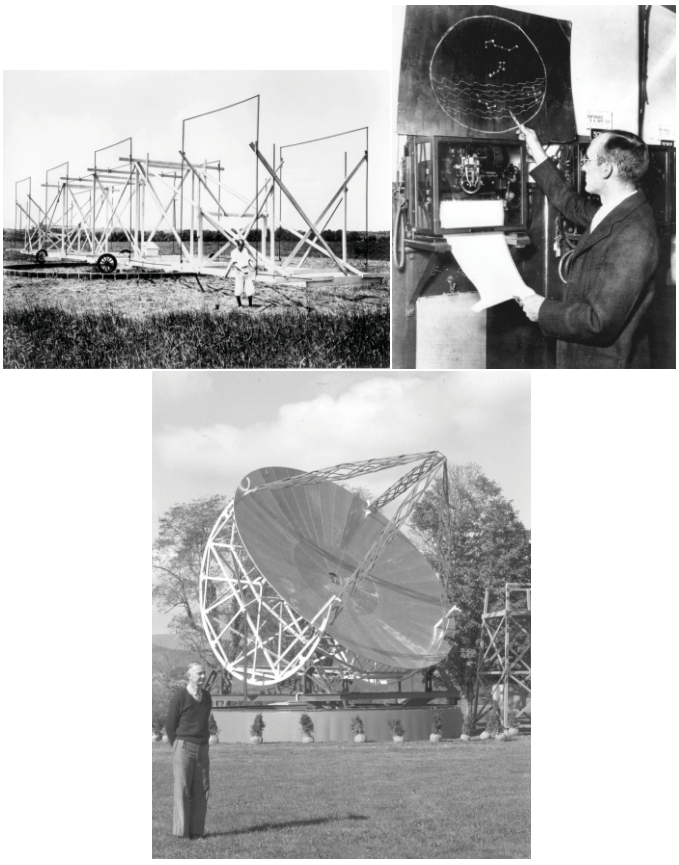

Figure 1. **Top Left**: Karl Jansky with his rotating antenna (Credit: NRAO/AUI/NSF). **Top Right**: Jansky points to the constellation of Cassiopeia on a sky map (Credit: NRAO/AUI/NSF). **Bottom**: Grote Reber with his reassembled backyard telescope built originally in 1937 (Credit: NRAO/AUI/NSF).

it is relevant for college students in India with interest in radio astronomy. The article is organized as follows: Section 2 gives a historical overview of radio astronomy and interferometry, Section 3 describes the SWAN initiative, and Section 4 illustrates radio imaging concepts using my work with the SWAN telescope.

2. A Brief History

Reber's telescope was the first-ever parabolic radio telescope and was considerably more advanced than Jansky's dipole array.

Radio astronomy practically started in the 1930s, when Karl Jansky used his rotating antenna and obtained evidence of static radio emission at 20.5 MHz from the direction of the Sagittarius constellation that repeated every sidereal day [1]. Inspired by

Jansky's work, Grote Reber used his backyard telescope to obtain evidence of radio emission from the Milky Way galaxy at 160 MHz [2]. Though there were several independent, successful attempts to detect solar radio waves, Reber was the first to publish his findings on the same. Following WWII, scientists started building bigger and better telescopes to study the radio emission from the Sun and other astronomical sources. Over the years, this has branched out to the study of other radio sources such as radio galaxies, quasars, pulsars, and masers.

Most gases in galaxies, though invisible to optical telescopes, can be seen by radio telescopes. Fast moving electrons, neutral atoms and molecules emit radiation at radio frequencies. In 1951, Ewen and Purcell discovered a spectral line emission from neutral hydrogen at 21 cm, which has far-reaching consequences in cosmology [3]. The discovery of the cosmic microwave background radiation, regarded as evidence for the Big Bang theory, was made through radio astronomy by Penzias and Wilson using their 6 m horn antenna [4]. In 1967, Jocelyn Bell, a graduate student at Cambridge University, working with Dr Anthony Hewish, detected repeating pulses from the sky, which were later attributed to a new category of sources called pulsars [5].

Radio waves from astronomical sources are extremely weak by virtue of the very large distance, and hence it is necessary to concentrate radio waves from a large area into a small feed placed at the focus of a reflecting dish. But in the case of radio astronomy, we face a slight problem. We know that the diffraction limit of a single telescope is roughly $\theta \sim \frac{\lambda}{d}$ where λ is the wavelength of the incoming light, and d is the diameter of the telescope we are observing with. Since radio wavelengths are very large, in order to get a reasonably good angular resolution, we need to build huge telescopes. But mechanical and maintenance problems come into play beyond a certain aperture size, and it becomes challenging to construct steerable structures with diameters beyond a certain limit. This is precisely where radio interferometry comes in.

For example, if we wish to get 1 arcsec angular resolution at 20 cm wavelength, we would need to build a dish that is 40 km in size!

2.1 *Radio Interferometry*

A very nice introduction to radio interferometers is available in the "*Essential Radio Astronomy*" course by NRAO [6].

Radio interferometry is a technique in which multiple antennas, placed at different locations on the surface of the Earth, are used coherently to mimic a radio telescope of a larger diameter. The simplest radio interferometer consists of two elements separated by some distance, which record the amplitude and phase of the radio waves coming from the sky. The input source voltages are multiplied together and time-averaged in a correlator. If both the telescopes track a source continuously, the delay is constantly changing. This can be visualized as a fringe pattern on the sky through which the source moves due to the Earth's rotation. The output of the correlator depends on how the source structure and the fringes are aligned with respect to each other. Long baselines (vectors connecting the two elements in an interferometer) record information about the small-scale structure of the source, while short baselines are sensitive to the large-scale structure (in the direction of the baseline). The combination of many elements placed at different positions allows a faithful reconstruction of an image of the source.

A sea interferometer uses just one antenna. The reflected ray from the surface of the sea gives rise to a virtual second antenna.

Interferometric techniques had been used in the domain of optical astronomy in the 1920s when the Michelson stellar interferometer was used to determine stellar radii. The first radio interferometer, however, was used by Ryle and Vonberg in 1946 [7], which consisted of arrays of dipole antennas observing at 175 MHz with the antenna beam pointing along the meridian while rotation of the Earth provided the necessary scanning across the right ascension. The earliest published record of the method of modern synthesis imaging is found in a paper by McCready et al. in 1946 [8], where they used the sea interferometer to obtain interference fringes. They even recognised that they were recording a single Fourier component of the brightness distribution (also called a visibility) and that a large number of antennas with different baselines would allow a complete Fourier synthesis. This is the basis of what is now known as aperture synthesis. Another significant advancement in the field of synthesis imaging was the method of Earth rotation aperture synthesis, used first by O' Brien in 1956

[9], in which the rotation of the Earth is utilised to obtain a higher sampling of the spatial frequency space.

3. The SWAN Initiative

The SWAN is a strategic initiative at the Raman Research Institute (RRI), and it proposes the design, development and use of a broadband radio interferometric array across India. The main objectives of the initiative are:

- The SWAN will conduct searches and studies of transient radio sources.
- It will be used to conduct high-resolution imaging of astronomical sources at low radio frequencies as Indian VLBI (Very Long Baseline Interferometer).
- The initiative will involve a large number of undergraduate and postgraduate students and provide them opportunities to actively participate in the development as well as in research using the array network. Moreover, through the training of students, it becomes a feeder for the SKA and other radio observatories.

A description of the requirement and motive behind the SWAN is available on the SWAN website [10].

3.1 *Current Setup of SWAN*

The SWAN uses an array of MWA (Murchison Wide-field Antenna) [11]. In the SWAN setup, the antennas are placed in the same arrangement as in the MWA radio telescope. 16 crossed dipole antennas arranged in a 4×4 matrix placed on a conducting wire mesh constitute a single tile (*Figure* 2). In Phase 0 of SWAN, 7 such tiles are placed in different locations at the Gauribidanur radio observatory.

3.2 *Pointing a SWAN Tile*

Since a SWAN tile consists of an array of fixed antennas, the pointing needs to be done electronically. When the source is situated exactly at the zenith, the incoming wave-front reaches all the

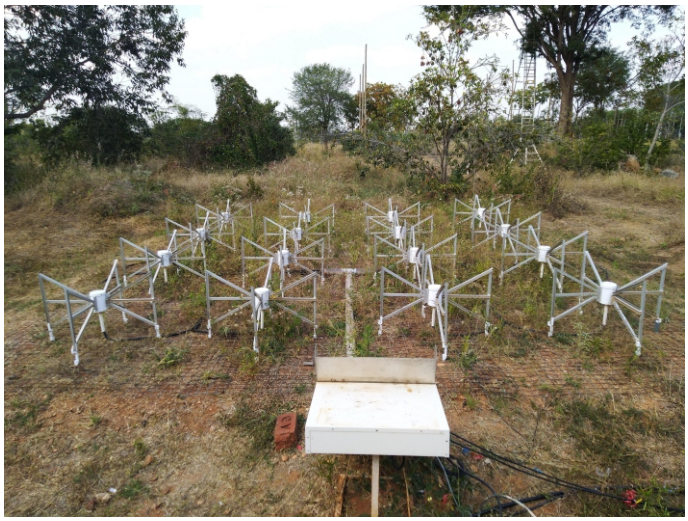

Figure 2. A single SWAN tile containing 16 Murchison Wide-field Antennas. The white box seen in the image is the beamformer.

antennas in a tile at the same instant, and the signals for each polarization can be added readily. However, if the source is situated at some angle from the zenith, the antennas closer to the source will receive the signal earlier, while those away from the source will receive the signal with some time delay. This is illustrated in *Figure* 3. Hence it is necessary to introduce delays so that the measurement of the intensity of the source can be made assuming that all the antennas are receiving an equal amount of photons at the same instant of time. This is done by the beamformer [11]. The beamformer takes two input signals for each antenna and introduces the appropriate delays electronically in order to phase the tile in the direction of the source we wish to observe.

3.3 *Processing of the Signals*

The output wires from the beamformer reach the control room, which contains several units for processing the signal and storing the data. These consist of the RF-IF block, DSP block, LO block, GPS block and the DASs (Data Acquisition Systems). Each DAS records raw voltage time sequences corresponding to 16 MHz bandwidth for each channel and stores the data in a binary file. A detailed description of the SWAN system is available at [12].

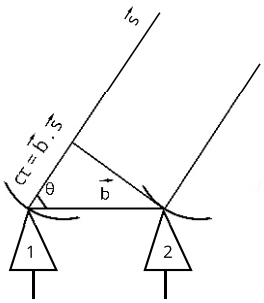

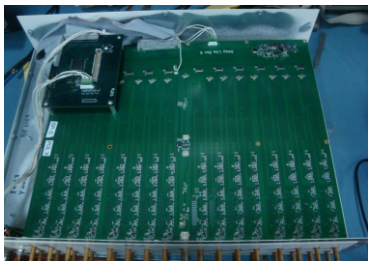

Figure 3. **Left:** Since two antennas are separated by some distance, a plane wave-front reaches the two antennas with some time difference given by $\tau = \frac{\vec{b}\cdot\vec{s}}{c}$ where $\vec{b}$ is the vector connecting the two antennas, $\vec{s}$ is the source vector and c is the speed of light. This delay is corrected by the beamformer by applying appropriate delays electronically to the signals from the antennas before adding the signals from all antennas corresponding to the same polarization. **Right:** The inside of a beamformer. The long wires necessary for introducing the delays can be seen.

4. Data Analysis Using SWAN

For initial familiarity with data analysis, the SWAN students are encouraged to work on a piece of processed Vela pulsar data obtained using the Ooty Widefield Array. It is a two column data (each corresponding to a sub-aperture), and the exercise involves the computation of the dynamic power and cross spectra followed by an attempt of incoherent dedispersion. Once the students are comfortable with two column pulsar data, they are encouraged to play with Green Bank Telescope raw data of the Crab pulsar since the data format is exactly the same as that obtained in SWAN (.mbr format [13]). A report describing some of the analysis is available at [14].

A few useful links for getting started with radio astronomy and data analysis are given as follows: reference material [15], Vela data and analysis steps [16], a sample of SWAN data [17].

4.1 *Synthesis Imaging*

This section describes the analysis I did to implement deconvolution algorithms on simulated images using Python.

4.1.1 Background: The elements in a radio interferometric array are used to sample the visibility space at discrete spatial frequencies, which depend upon the projections of the baseline vectors on the plane perpendicular to the source vector. If there are N geometrically separated elements in an array, then $\frac{N(N-1)}{2}$ baselines and hence the same number of spatial frequencies can be sampled

This projection is given by: $\vec{b}_{proj} = \vec{b}$ - $(\vec{b}.\vec{s})\vec{s}$, where $\vec{b}$ and $\vec{s}$ are the baseline and source vectors respectively. Then the required u and v coordinates are $\frac{\vec{b}_{proj}\cdot\vec{u}_{basis}}{\lambda}$ and $\frac{\vec{b}_{proj}\cdot\vec{v}_{basis}}{\lambda}$, where $\vec{v}_{basis}$ = projection of vector pointing towards North Celestial Pole on this plane.

by the array. But as the Earth rotates, the length and direction of the baselines projected on the plane perpendicular to the source changes. Hence, if we record voltages for a long period of time, a large number of samples in the spatial frequency space can be obtained by the array. This method is known as Earth rotation aperture synthesis.

Now, if V_{pq} is the complex visibility measured by the baseline "pq" as a function of u and v coordinates (which, in turn, change with time), and I_ν represents the intensity distribution in the sky as a function of direction cosines l and m, then the observed sky and the sampled visibilities have a Fourier pair relationship via the Van Cittert–Zernike theorem:

$$V_{\mathrm{pq}}(u, v, 0) = \int_{-\infty}^{\infty} \int_{-\infty}^{\infty} I_\nu e^{-2\pi i(ul+vm)} dldm.$$

The visibilities are nothing but complex cross-correlations of the signals received by two elements of the array, corrected for the geometric delay. Hence, once we obtain the voltages measured by the elements in an interferometric array, we have to correct for the geometric delay between the elements at every instant. Then the complex cross-correlations for each of the $\frac{N(N-1)}{2}$ pairs of elements need to be computed at every time point after suitable integration. Since we know how the projections of the baselines change with time, we can grid the data on a 2D matrix, the value at position (u, v) representing the visibility corresponding to projected baseline components u and v. The inverse Fourier transform of the matrix should give us the dirty image obtained using the interferometer.

4.1.2 CLEANing the image: Since we have not sampled the entire visibility space using the array, the image produced in this way is not a true representation of the radio sky. The relationship between the true sky image and the dirty image obtained from sampled visibilities is given by:

$$I_{\mathrm{dirty}} = B_{\mathrm{dirty}} \circ I_{\mathrm{true}}.$$

(where I_{dirty} is the dirty image, I_{true} is the true sky image, $\circ$ denotes a convolution and $B_{\mathrm{dirty}} = \mathcal{F}^{-1}(S_{\mathrm{uv}})$ where S_{uv} is the UV

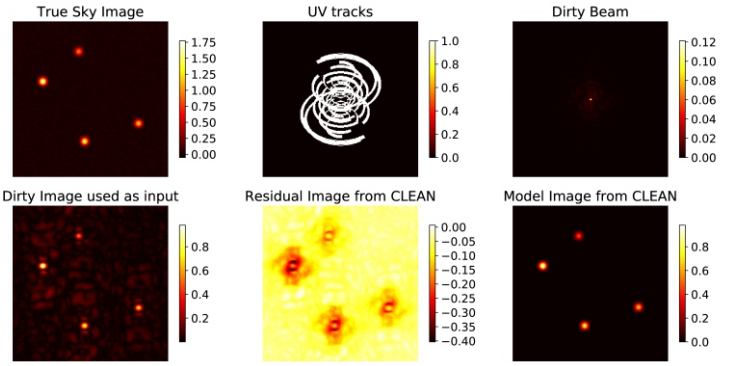

Figure 4. Results of implementation of Clark algorithm with same parameters. It seems give better results than the Hogbom algorithm and the faintest source (on the top right) is recovered more distinctly in the final image.

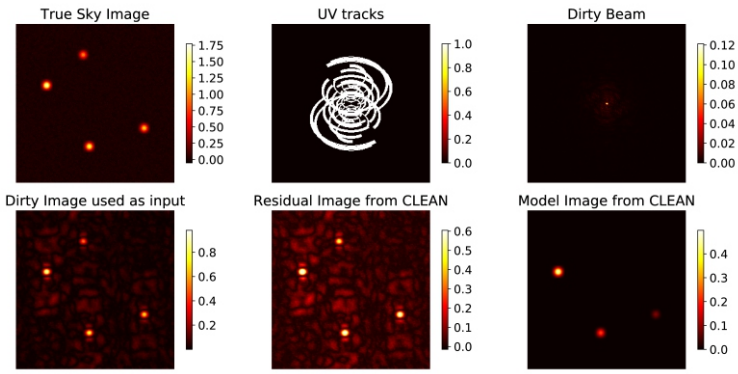

Figure 5. Results obtained from implementation of Hogbom algorithm on simulated images with noise. The uv plot assumes the SWAN tile configuration with the source at RA = 45°, Dec = 45°.

sampling function)

Hence, knowing the coordinates of the elements in the array, we can simulate the sampling pattern and compute its inverse Fourier transform to obtain the dirty beam. We can obtain the dirty image by gridding the sampled visibilities and computing its inverse Fourier transform. We know that the true sky image convolved with the dirty beam produces the dirty image. We now want to estimate what the true sky image looks like, and this process of obtaining the true sky image from the dirty image (obtained due to incomplete sampling) utilizing the dirty beam (containing information about how bad our sampling was) is called deconvolution. There are several algorithms that can be used to perform

iterative deconvolution on radio images. I tried to implement two of these, namely, the Hogbom and Clark methods, in this analysis, on a simulated image containing four Gaussian sources with some level of noise. In the analysis, both the Hogbom and Clark algorithms were implemented with the same number of iterations.

4.1.3 Comments: Though the Hogbom and Clark algorithms perform the deconvolution in essentially the same procedure, the Clark algorithm is considerably faster and can recover all four simulated sources (*Figure* 4), which the Hogbom is unable to do with the same number of iterations (*Figure* 5).

4.2 *Delay Calibration*

A crucial first step in radio imaging is the estimation and correction of geometric delays between the signals received by different tiles before the cross-correlations are computed.

4.2.1 Background: The radio waves from a celestial object do not fall on all the tiles simultaneously (unless the object is at its zenith), and hence there is a delay in the arrival times at any two tiles. This delay leads to a linear phase gradient across the frequency channels. As the Earth rotates, the geometric delay between the tiles changes and hence the phase gradient changes. If the RA and Dec of the object, tile coordinates, observation date and time, and central frequency of observation are known, then we should be able to simulate how the delay and phase are expected to change with time due to the Earth's rotation. This can be cross-checked with the observed delay changes from the data. If the residual delays show a trend, then it can be interpreted as arising due to the lack of accuracy of the tile coordinates that were used to simulate how the delays should change with time.

4.2.2 Data used: The data used for the analysis were 1-hour observations of the Sun taken using the SWAN on 20/02/2017 at a central frequency of 200 MHz. Four DASs (data acquisition systems) were active during the observations. Also, the two channels of a das, instead of being connected to the two polarization components of the same tile, were connected to the same polarization

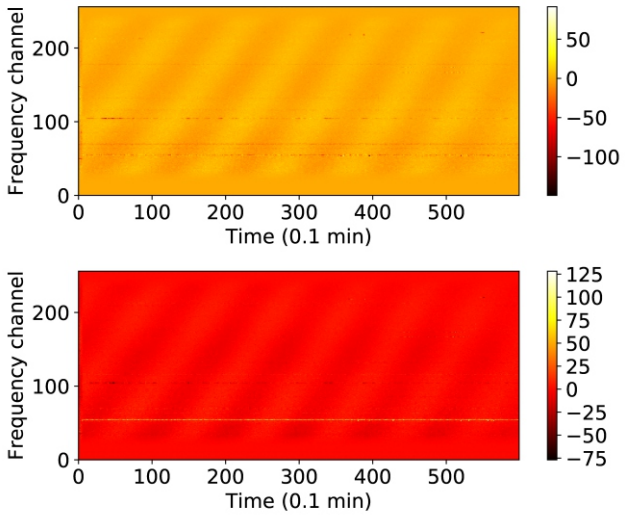

Figure 6. Real and imaginary parts of dynamic cross spectra for one pair of tiles.

component of two different tiles so that the cross-correlations can be computed without the need for synchronization.

4.2.3 Selecting integration time: In order to build up the signal-to-noise ratio (SNR), the data needs to be integrated for some time. But too high an integration time may lead to bandwidth decorrelation due to uncompensated delay from sources near the edge of the beam. Hence selecting the appropriate integration time is very important in order to get the maximum SNR without losing too much information. So we need to know how fast the correlation is changing and, given that we have compensated for the central direction, what should be the maximum integration time such that sources farthest from the centre of the beam do not cause decorrelation due to uncompensated delay.

4.2.4 Dynamic cross spectra: The cross-correlation between two signals describes the level of similarity between the two signals, and dynamic cross spectra are nothing but the cross spectra as a function of time. Now, the output of a two-element interferometer tracking a source is a fringe pattern in the sky. Hence, if the tiles are actually recording data from the same source, we should see slanted fringes in the dynamic cross-spectrum plot since the

The cross-correlation between two signals describes the level of similarity between the two signals, and dynamic cross spectra are nothing but the cross spectra as a function of time.

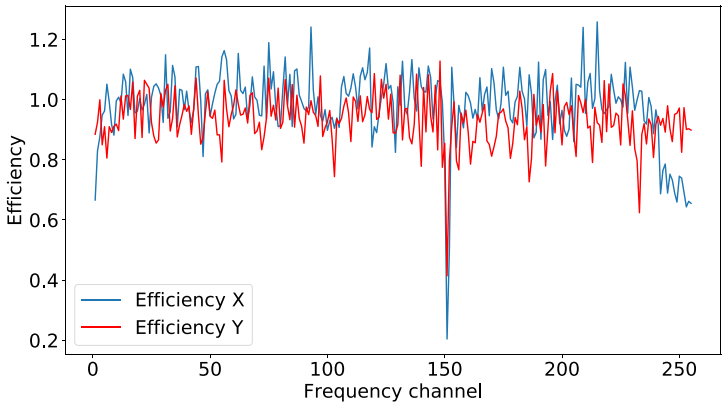

Figure 7. Plot of efficiency vs. frequency channel for a piece of SWAN data. The dips indicate the channels affected by RFI.

geometric delay gives rise to a phase gradient across frequency (*Figure* 6).

4.2.5 RFI mitigation: The signal received by the antennas may contain radio frequency interference (RFI) produced by local sources apart from the signal from the sky. The RFI are usually restricted to a few frequency channels, and hence it can be removed by going to the frequency domain and removing the frequency channels affected by RFI. But in order to remove them, we first need to identify the RFI-affected channels [18].

Here, we make the assumption that the signal from the sky is purely Gaussian, and hence the intensities follow an exponential distribution. We know that in exponential distribution, $\frac{\mu}{\sigma} = 1$, where μ = mean, σ = standard deviation.

Now, we take the observed mean as a proxy for the expected standard deviation and define efficiency (E) as:

$$E = \frac{\mu}{\sigma\sqrt{TBP}},$$

where TBP = time bandwidth product.

This definition can be justified as follows: Suppose we average for 'N' packets, then the mean remains the same, but the standard deviation reduces by $\sqrt{N}$. The time-bandwidth product is N. If

the signal is from the sky, then the mean should equal the standard deviation before averaging. After averaging, $\mu = \sqrt{N}\sigma$. Hence, the calculated efficiency should equal 1. For RFI, $\mu < \sqrt{N}\sigma$ and the calculated efficiency should be less than 1. During the analysis, the efficiency of each frequency channel in the frequency domain is calculated for individual power spectra (*Figure* 7). The dynamic spectra are produced after integration and RFI-affected channel rejection.

The following logic was adopted to select the threshold efficiency below which a channel should be rejected. Suppose the ensemble size for which mean and rms are computed is M. Then the uncertainty in $\frac{\mu}{\sigma}$ is $1/\sqrt{M}$. A Gaussian is constructed for each channel whose standard deviation equals the rms of the channel across time. Now, if we have k frequency channels, we find the minimum value of 'a' such that P($|x|$ > aσ) < $\frac{1}{k}$. Now, this 'a' should reflect the confidence level in our efficiency calculation. Hence, a channel should be rejected if its efficiency is less than: (1 - $\frac{a}{\sqrt{M}}$).

4.2.6 Estimating observed delay using Hilbert's transform: Here, we make use of the cross correlation theorem which states that: a $\otimes$ b = $\mathcal{F}^{-1}$ ($\mathcal{F}(a)^*\mathcal{F}(b)$) (where $\otimes$ denotes cross correlation, $\mathcal{F}$ denotes Fourier transform and A^* = complex conjugate of A).

During the analysis, we first compute the FFT (fast Fourier transform) of the signals from two tiles and find their complex cross-correlations (AB*) in the frequency domain. Then we retain only the positive frequencies so that we get the analytic signal corresponding to the cross-correlation function upon inverse Fourier transform (*Figure* 8). This whole procedure is equivalent to adding the signal x(t) with i$\mathcal{H}$[x(t)] (where $\mathcal{H}$[x(t)] is Hilbert's transform of x(t)), which has the same effect of filtering out the negative frequencies, giving rise to a complex-valued function after IFFT (inverse fast Fourier transform). Before IFFT, zero padding might be done to improve the accuracy of finding the peak position in the cross-correlation function. Now, the delay can be found just by noting the peak position in the cross-correlation function. But since our sampling frequency is finite, we cannot track the peak as

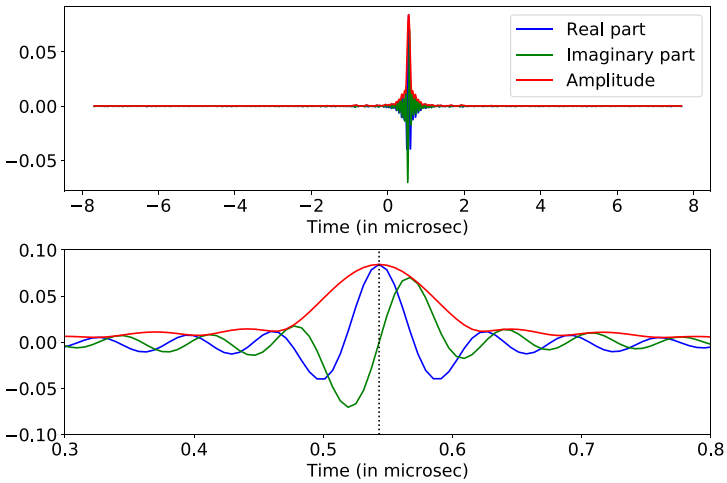

Figure 8. The complex cross-correlation function obtained using a piece of simulated Gaussian noise and a shifted version of the same data. The position of the peak of the amplitude indicates the shift. The bottom panel shows a zoomed version of the plot.

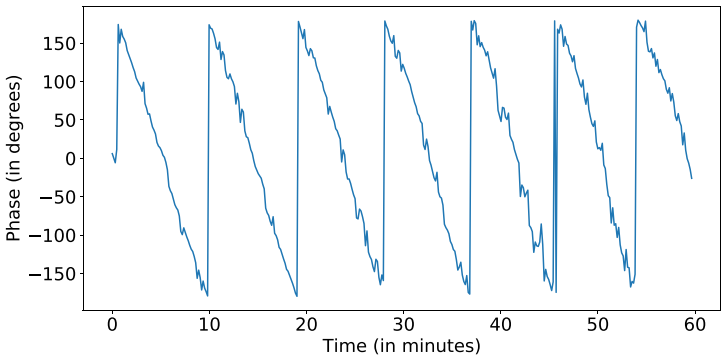

Figure 9. Variation of phase with time as the source moves through the sky obtained by using SWAN data from two tiles.

it moves between two sampling points. This gives rise to discrete jumps in the plots of delay against time obtained in this manner. In a much better approach, the phase at the peak can be found by computing the value of $\tan^{-1}\left(\frac{\text{Imaginary Part}}{\text{Real Part}}\right)$ at the peak.

This value of phase is then monitored for every averaged spectrum and results in a saw-tooth-like function of the phase vs. time (*Figure* 9). The 360° wraps are removed, and each value is divided by the central frequency of observation to get the plot of

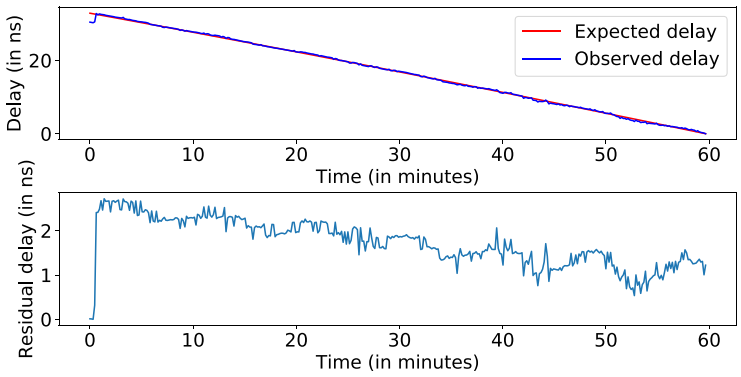

Figure 10. Variation of simulated, observed and residual delays (obtained through phase estimation) with time.

delay against time.

4.2.7 Residual delays: In order to calculate the residual delays, first, a phase gradient (corresponding to the value of the expected delay) was applied to the cross-spectrum, followed by the same Hilbert's transform-based phase estimation on the resulting spectrum to get the residual delay values (*Figure* 10). The trends in the residual delay plots can be attributed to the lack of accuracy of the GPS coordinate measurements.

4.2.8 Application of delay estimation (apart from imaging): This method of delay estimation can be used to back calculate the sky coordinates of the source, which is giving rise to the observed delay trends. The delay trends for each baseline will give rise to an imaginary annulus in the sky within which the source responsible for this delay should lie. The annulus is centred in the direction where the baseline points, and the width of the annulus corresponds to our uncertainty in measuring delays. If this analysis is repeated for multiple baselines, then the overlap of the corresponding annuli will give us a very good estimate of the source coordinates in RA, Dec space.

4.3 *SWAN Imaging Challenge*

The SWAN Imaging Challenge was conducted by RRI first in 2018 and again in 2019. The aim of the challenge was to produce a 100 square degree image of any part of the radio sky with maximum possible fidelity and angular resolution using the existing SWAN setup at Gauribidanur. A few versions of software for data reduction (developed by students) at least till the estimation of cross spectra were made available, along with some data obtained using the SWAN. In total, nineteen teams from institutes across India participated in the SWAN Imaging Challenge 2019, and six teams finally submitted their completed results. The submitted entries were sent to a jury panel consisting of four respected practising radio astronomers. The jury comments were passed to the respective teams, and in their unanimous verdict, the jury chose the entry from IISER Mohali Team 1 as the best effort and the winners of the SWAN Imaging Challenge 2019.

***4.3.1 Data used*:** For the analysis relevant to the imaging challenge, we used observations of the sun (target) obtained on 3rd February 2017 and observations of Cygnus A (primary calibrator) obtained on 15th December 2016. The observations were 4 hours long, and 4 tiles were active during the observations (*Figure* 11).

4.3.2 Selecting channel width: Since we are compensating for the geometric delay at the centre of the image, the delays from sources at the edge of the image remain uncompensated and give rise to bandwidth decorrelation. Since the difference in phase due to the source in two adjacent narrow spectral channels is proportional to the channel width, this gives rise to a constraint on the width of the channels.

4.3.3 RFI rejection and cross spectra: The analysis described in section 4.2.5 was used to identify the RFI affected frequency channels (which were flagged later). The dynamic cross spectra, described in section 4.2.4, were computed, and fringes could be seen for all baselines signifying that the source was actually seen during the observation.

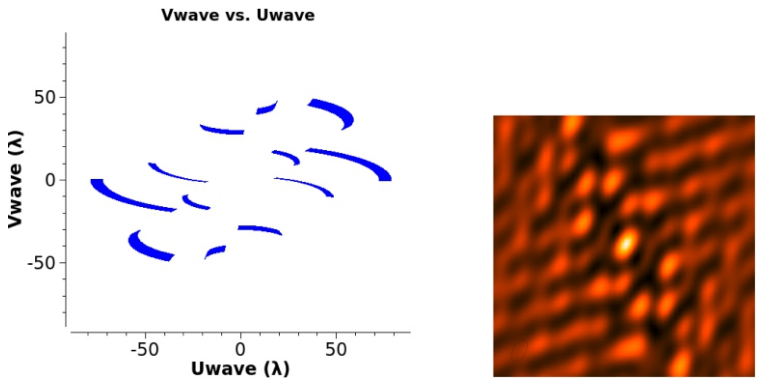

Figure 11. Left: The UV coverage for the tiles used in the analysis for the observation period. **Right**: The corresponding dirty beam.

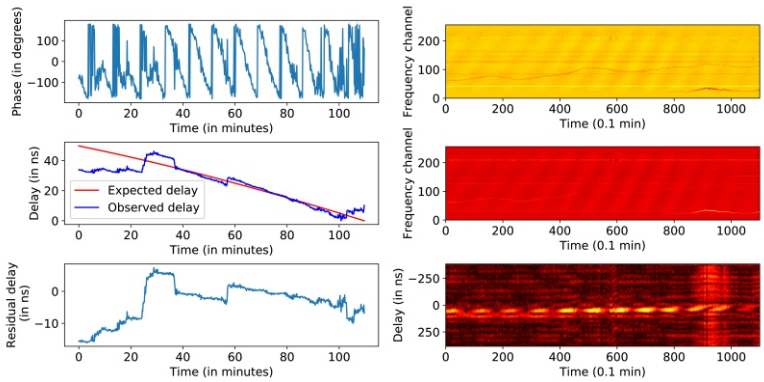

Figure 12. Results by running the software for delay calibration (described in section 4.2) on the imaging data for a pair of tiles for 2 hours. This was repeated for all 4 pairs. The plots describe phase (**top left**), delays (**centre left**), residuals (**bottom left**), cross spectra real part (**top right**), cross spectra imaginary part (**centre right**), and dynamic delay plot (**bottom right**).

4.3.4 Correcting for geometric delay: In order to produce an image, we need to obtain visibilities that are corrected for the geometric delay. So we need to generate the geometric delay values for each pair of tiles used during the observations. The analysis in section 4.2 was used to confirm that the expected delays generated by our software are close to the actual delay obtained from the data (*Figure* 12). In order to correct for the calculated geometric delay, the samples were shifted accordingly before cross-correlation up to a single sample delay. Any remaining fractional sample delay was accounted for by applying the corresponding phase gradients to each cross-spectrum.

4.3.5 Simulating observation using CASA: In order to utilize the

tasks for calibration and imaging available in the radio astronomy software CASA, it was necessary to import the data as measurement sets (.ms tables), which can be used readily in CASA. In order to avoid writing down the metadata carefully ourselves, the simulation feature in CASA was used to simulate a mock observation with the same parameters as the actual observation and using the tile coordinates of the SWAN. CASA produces a .ms table containing all the metadata, and the data column in it is then simply replaced by the computed corrected visibilities. This was repeated for both the source and calibrator. Later, a pipeline was developed that takes the SWAN data files (of both source and calibrator) and the observation parameters and returns a single .ms table that can be used in CASA with the source and calibrator data in different fields.

4.3.6 Calibration and imaging: The .ms table thus produced was taken as input in CASA, and CASA tasks were used to do the following: The calibrator data was used to calculate and solve for the system parameters and store the solutions in a calibration table. These solutions were then applied to our target field. The corrected data was then used to perform the gridding and CLEANing using the Hogbom method, and the parameters were varied until a smooth residual image was obtained (*Figure* 13).

5. SWAN Activities for Undergraduates

RRI conducts several activities throughout the year in which the students of institutes associated with SWAN are encouraged to participate. Every year, RRI conducts the "SWAN Hands-On Summer", in which undergraduate and postgraduate students from different institutes across India are given an opportunity to visit the Gauribidanur Radio Observatory. The students are given complete freedom to experiment with the instrumentation to understand the system, conduct tests and observations and learn radio astronomy techniques in general and the SWAN setup in particular. The students are also encouraged to follow up on their interests through remote access to the Gauribidanur computers.

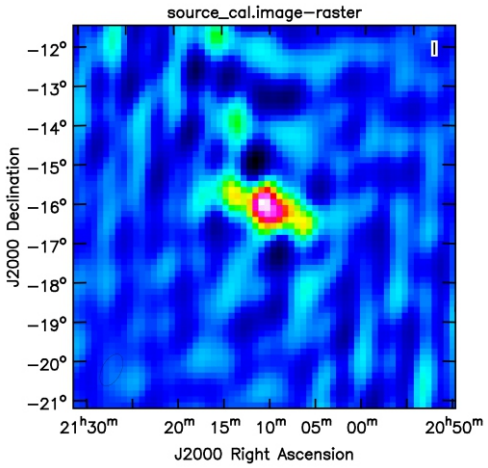

Figure 13. The final image obtained from the analysis for the imaging challenge.

There are often initiatives to observe relevant astronomical events using the SWAN in which students from associated institutes are encouraged to participate through remote access. On 27th September 2018, there was a coordinated observation of the Crab pulsar using telescopes in Australia and India, and the SWAN participated in this campaign. This provided an opportunity for the students to learn the analysis of SWAN data and make observations using the setup. On 19th September 2019, the occultation of the Crab by the moon was observed using the SWAN, and the data from the observation was made available to all the students for analysis. There are several online teleconferences and "busy weeks" organized throughout the year where the students learn the basics of radio astronomy and analysis of SWAN data.

Acknowledgements

I am grateful to Prof. Jasjeet Singh Bagla, Prof. Avinash Deshpande and Pavan Uttarkar for their valuable suggestions. I would also like to thank my team members for the SWAN Imaging Challenge: Devang Liya, Vishal Gaur, Nithishwer, Sarbani Chatterjee, Rahul Ramesh, Aabhas Gulati, Anshu, Kunal Verma, Anshuman Acharya and Utkarsh Pathak for their contributions during the competition.

Suggested Reading

[1] Karl G Jansky, Electrical disturbances apparently of extraterrestrial origin, *Proceedings of the Institute of Radio Engineers*, Vol.21, No.10, pp.1387–1398, 1933.

[2] Grote Reber, Cosmic static, *Proceedings of the IRE*, Vol.28, No.2, pp.68–70, 1940.

[3] Harold Irving Ewen, and Edward Mills Purcell, Observation of a line in the galactic radio spectrum, *Classics in Radio Astronomy*, pp.328–330, 1951.

[4] Arno A Penzias, and Robert Woodrow Wilson, A measurement of excess antenna temperature at 4080 Mc/s, *The Astrophysical Journal*, Vol.142, pp.419–421, 1965.

[5] Antony Hewish et al., Observation of a rapidly pulsating radio source, *Nature*, Vol.217, No.5130, pp.709–713, 1968.

[6] https://www.cv.nrao.edu/course/astr534/Interferometers1.html
https://science.nrao.edu/opportunities/courses/era/

[7] M Ryle, and D D Vonberg, Solar radiation on 175 Mc./s, *Nature*, Vol.158, No.4010, pp.339–340, 1946.

[8] L L McCready, Joseph Lade Pawsey, and Ruby Payne-Scott, Solar radiation at radio frequencies and its relation to sunspots, *Proceedings of the Royal Society of London. Series A. Mathematical and Physical Sciences*, Vol.190, No.1022, pp.357–375, 1947.

[9] P A O'brien, The distribution of radiation across the solar disk at metre wave-length, *Monthly Notices of the Royal Astronomical Society*, Vol.113, No.5, pp.597–612, 1953.

[10] http://www.rri.res.in/SWAN/SWANRRI.html

[11] Colin J. Lonsdale et al, The murchison widefield array: Design overview, *Proceedings of the IEEE*, Vol.97, No.8, pp.1497–1506, 2009.

[12] http://bit.ly/swan_asi_poster

[13] Yogesh Maan et al., RRI-GBT multi-band receiver: motivation, design, and development, *The Astrophysical Journal Supplement Series*, Vol.204, No.1, pp.12, 2013.

[14] http://bit.ly/swan_pulsar_report

[15] http://bit.ly/swan_reference_material

[16] http://bit.ly/swan_vela_analysis

[17] http://bit.ly/swan_sample_data

[18] Avinash Deshpande, Correlations of spectral intensity fluctuations: Application to radio frequency interference mitigation, *Radio Science*, Vol.40, No.05, pp.1–9, 2005.

Address for Correspondence
Satyapan Munshi
81A, K.P. Roy Lane
Kolkata 700 078, India.
Email:
satyapan.iiserm@gmail.com